Progress of Theoretical Physics, Vol. 81, No. 2, February 1989

Temporal Intermittency in the Energy Cascade Process and Local Lyapunov Analysis in Fully-Developed Model Turbulence

Koji OHKITANI and Michio YAMADA*

Department of Physics, Kyoto University, Kyoto 606
**Disaster Prevention Research Institute, Kyoto University, Uji 611*

(Received August 25, 1988)

Energy cascade process is investigated numerically on a scalar model of fully-developed three-dimensional turbulence. It is found that energy propagates through the inertial range intermittently like bursts which are separated by quiescent periods (Siggia's view revisited). During the activated phase the first *local* Lyapunov exponent oscillates violently, and the support of the first Lyapunov vector spreads over the inertial subrange.

§ 1. Introduction

Various turbulent phenomena observed in diverse fields of nonlinear physics have their origin in strange attractors in the phase space. One of the most important examples of such phenomena is fully-developed three-dimensional (3D) turbulence governed by the Navier-Stokes equation, where the phase space is an infinite dimensional function space and the strange attractor has a huge dimension. Since its discovery, the concept of the strange attractor has been expected to give a unified approach to the turbulent phenomena.[1] However, up to now, the notion of the strange attractor is useful mainly for lower-dimensional turbulent motions, and has not yet given a satisfactory understanding of fully-developed turbulence. Particularly, no interpretation is found for the fundamental scaling law of Kolmogorov in the theory[2] of chaotic dynamical systems. This is firstly because the fully-developed turbulence has much more degrees of freedom than the present-day supercomputers can reasonably deal with, and secondly because most of the characterizations of strange attractors devised so far are practically applicable to systems with small degrees of freedom. At present, at least from a numerical point of view, the fully-developed turbulence seems to be still beyond the approach of the methods in the dynamical system theory.

Recently, a certain class of cascade models of turbulence has been proposed to fill in this gap. The cascade model of this kind has a tractable dimension, and shares some fundamental aspects with fully-developed 3D Navier-Stokes turbulence; especially it has the Kolmogorov scaling property (K41) of the temporally averaged energy spectrum in its *chaotic* state. It is, therefore, of some interest to examine this tractable model in detail by the methods in the dynamical system theory. In previous papers[3),4)] we discussed the scaling properties of both the energy spectrum and the Lyapunov exponents in the cascade models. (These results are summarized in the following section.) What we were concerned there with were temporally averaged properties, for example, the mean model energy in wavenumber space and the mean

divergence rates of nearby trajectories in the phase space. In this paper we are interested in the fluctuations around these averaged properties. We consider fluctuations of energy transfer and of local Lyapunov exponents, and seek possible relationships between these fluctuations. The former is the fluctuation of the energy cascade rate and is directly related to the K41 theory, while the latter reflects a local characteristic of the chaotic trajectory. The relation between the temporal intermittency in the energy cascade process and the local property of the chaotic motion is the subject of this paper.

We briefly review in § 2 the model equation together with the scaling properties of the energy spectrum and Lyapunov spectrum. In § 3 the energy cascade process is investigated in some detail with emphasis on its temporally intermittent structure. We examine in § 4 the local Lyapunov exponents as a measure of temporal intermittency in the Lyapunov perspective and behaviors of the Lyapunov vectors are described. These two sections are the main part of this paper, where temporal intermittency is characterized both from the Fourier and the Lyapunov perspective. Section 5 is devoted to a summary and discussion.

§ 2. Basic properties

In this section we present the chaotic cascade model with numerical procedures which we employ in this paper. We summarize our previous papers[3),4)] on its basic properties for the convenience of later discussion.

2.1. *Chaotic cascade model*

Several kinds of cascade models have been proposed so far,[5)] but most of them do not embody intrinsic stochasticity, i.e., chaotic behavior of their solution. The Navier-Stokes equation, on the other hand, does have intrinsic stochasticity, and physical quantities of real turbulence gain their importance only after they are averaged in some sense. This observation suggests that a cascade model with intrinsic stochasticity (chaotic cascade model) provides useful information about the dynamical structure of turbulence. To the authors' knowledge, such chaotic cascade model was first proposed (for 3D MHD turbulence) by Grappin and coworkers,[6)] who found that the time-averaged energy spectrum and the Lyapunov dimension of the attractor have the same scaling property as in the K41 theory. A similar model with a stochastic solution has also been discussed by Orszag.[7)]

In the following in this paper we treat a cascade model proposed for 3D Navier-Stokes turbulence.[3)] The model is in a sense a complex version of a model for (2D Navier-Stokes turbulence) first proposed by Gledzer[8)] and later shown by Yamada and Ohkitani[9)] to have intrinsic stochasticity. The model for 3D turbulence is constructed in a discretized wavenumber space $\{k_n | k_n = k_0 q^n,\ n = 1 \sim N\}$. The velocity is represented by a set of complex variables $\{u_n\}$, where u_n stands for the velocity components whose wavenumber k satisfies $k_n < |k| < k_{n+1}$. The energy E and enstrophy Q are therefore defined as $E = \sum_n |u_n|^2/2$ and $Q = \sum_n k_n^2 |u_n|^2/2$, and the energy spectrum as $E(k_n) = |u_n|^2/(2k_n)$. Note that the phase space is a real $2N$-dimensional space $\{u_n^R, u_n^I\}$, where we define the innerproduct of $\{u_n = u_n^R + iu_n^I\}$ and $\{v_n = v_n^R + iv_n^I\}$ as

$\sum_{j=1}^{N}(u_j^R v_j^R + u_j^I v_j^I)$.

Each evolution equation for u_n is assumed quadratically nonlinear and coupled with nearest and second-nearest neighbors in the wavenumber space. The phase volume conservation $\sum_n(\partial \dot{u}_n^R/\partial u_n^R + \partial \dot{u}_n^I/\partial u_n^I)=0$ is assumed to hold, where dot denotes time derivative. These requirements are satisfied by the following equation:

$$(d/dt+\nu k_n^2)u_n = i[c_n^{(1)}u_{n+1}^* u_{n+2}^* + c_n^{(2)}u_{n-1}^* u_{n+1}^* + c_n^{(3)}u_{n-1}^* u_{n-2}^*] + f\delta_{n,4}\,, \tag{2·1}$$

where $*$ denotes the complex conjugate, f is a time-independent forcing term, ν is the kinematic viscosity, δ is Kronecker's δ and t is the time. Requiring further the detailed conservation of energy, we determine the real constants $c_n^{(1)}$, $c_n^{(2)}$, $c_n^{(3)}$ as follows:

$$c_n^{(1)}=k_n,\quad c_n^{(2)}=-\beta k_{n-1},\quad c_n^{(3)}=(\beta-1)k_{n-2}\,,$$
$$c_1^{(2)}=c_1^{(3)}=c_2^{(3)}=c_{N-1}^{(1)}=c_N^{(1)}=c_N^{(2)}=0\,, \tag{2·2}$$

where β is a real parameter. It can be shown that for $\beta>1$, Eq. (2·1) with $\nu=f=0$ conserves $\sum_{j=1}^{N}k_j^{\alpha}|v_j|^2$ ($\beta=1+1/q^{\alpha}$) in addition to energy. Here we take $\beta=1/2$ so that we have no other constraints other than energy.

The parameters used are $q=2$, $N=24$, $\nu=10^{-8}$, $k_0=2^{-4}$, $f=(1+i)\times 5\times 10^{-3}$. Time marching was performed by the fourth-order Runge-Kutta method with time step $\Delta t=10^{-4}$. The computation was carried out in the double-precision arithmetic on a vectorial computer VP-400 at Kyoto University.

2.2. *Kolmogorov's scaling law*

Starting from an appropriate initial condition, we solved Eq. (2·1) numerically. After a transient period, an unsteady but statistically stationary state is observed. The statistical quantities we discuss below are concerned with this stationary state.

According to the K41 theory,[2] statistical quantities in the inertial range are described by two parameters; the viscosity ν and the energy dissipation rate ε. In particular, the energy spectrum $E(k)$ is expressed as

$$E(k)=\varepsilon^{1/4}\nu^{5/4}E_e(k/k_d)\,, \tag{2·3}$$

where $k_d=\varepsilon^{1/4}\nu^{-3/4}$ is the dissipation wavenumber and E_e is a non-dimensional function. In the inertial subrange, Eq. (2·3) takes the well-known ν-independent form

$$E(k)=C\varepsilon^{2/3}k^{-5/3}\,, \tag{2·4}$$

where C is a universal constant.

Figure 1 shows the time-averaged energy spectrum obtained in the model equation (2·1). The power-law behavior is seen with the exponent $-5/3$. Also runs with several values of viscosity confirm the scaling law of the energy spectrum (2·3). Figure 2 shows the energy flux function $\Pi(k)$, defined by $\Pi(k_n)=\langle\sum_{j=n}^{N}u_j\dot{u}_j\rangle^*$ where the bracket denotes the time-average. The flux is fairly constant over the wavenumber range where the spectrum behaves as $k^{-5/3}$. We note that this constant energy

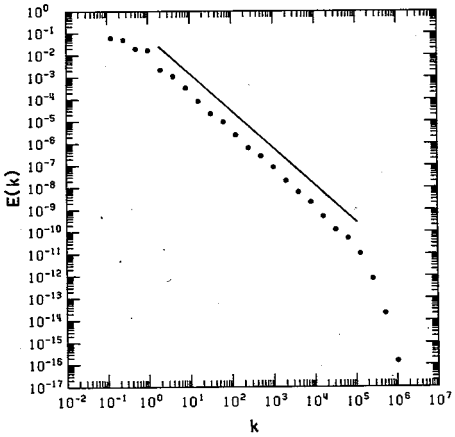

Fig. 1. The time averaged energy spectrum. The straight line shows the slope $-5/3$.

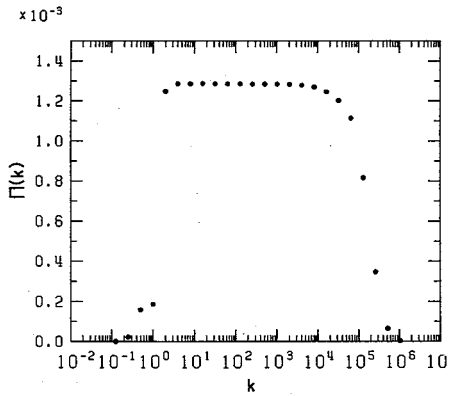

Fig. 2. The time averaged energy flux function.

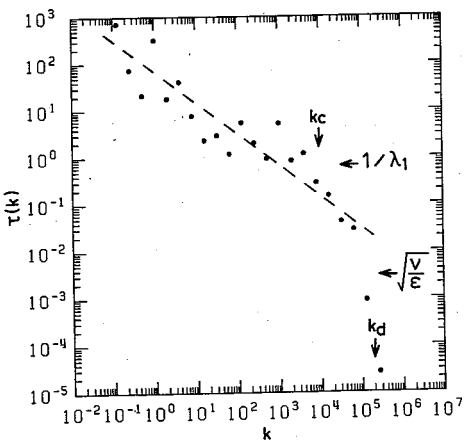

Fig. 3. The eddy turnover time (nonlinear time-scale) estimated as $\tau(k)=\sqrt{\langle(u(k)/\dot{u}(k))^2\rangle}$. The dashed line shows slope $-2/3$.

transfer rate is approximately equal to the dissipation rate $\varepsilon=2\nu Q=1.29\times10^{-3}$, which indicates statistical stationarity of the model turbulence. We also show in Fig. 3 the nonlinear time scale (or the turnover time) $\tau(k)$ defined by $\tau(k_n)=\sqrt{\langle(u_n/\dot{u}_n)^2\rangle}$.*) Although the fluctuations are noticeable, the result is consistent with $\tau(k)\sim k^{-2/3}$ in the inertial subrange, which is predicted by the scaling argument of K41 type. In the far dissipation range $\tau(k)$ falls off more rapidly than algebraically. All of these results show that the present model satisfies the K41 scaling law and thus deserves closer investigation.

2.3. *Lyapunov analysis*

We now employ the methods of Lyapunov analysis to characterize the motion governed by Eq. (2·1). Note that the result described in this section is related to the long-time averages and should be distinguished from local Lyapunov analysis, which is discussed in § 4 and is concerned with instantaneous behavior of solution.

Thanks to the intermediate size of the present model, we can compute all the Lyapunov exponents $\{\lambda_j|j=1\sim N\}$ (Lyapunov spectrum) by the standard method of Gram-Schmidt orthonormalization. In every case we treated, some of the Lyapunov exponents are positive, which demonstrates that the motion is chaotic and is due to a strange attractor. We plot the cumulated Lyapunov exponents in Fig. 4, taking j as abscissa and $\sum_{i=1}^{j}\lambda_i$ as ordinate. Several quantities can be computed from this; the maximum Lyapunov exponent $\lambda_1=1.54$, Kolmogorov-Sinai entropy (=sum of positive

*) The time-derivative $\dot{u}_n$ has been evaluated from nonlinear terms only.

λ_j's) $H=3.95$, and the Kaplan-Yorke dimension $D=29.8$.

The Lyapunov analysis has been done for several values of viscosity, and it is found[6),3)] that λ_1 (and H also) is proportional to $\nu^{-1/2}$. This may be taken to mean that λ_1 is proportional to $\sqrt{\varepsilon/\nu}$, the reciprocal of the eddy turnover time estimated at $k=k_d$. However the former is about 10^2 times smaller than the latter ($\sqrt{\varepsilon/\nu}=358.4$). It turns out that the value of λ_1 is closer to that of the reciprocal of the eddy turnover time estimated at $k_c\sim10^4$, the highest wavenumber with constant energy flux (Fig. 2). This wavenumber is about ten times smaller than k_d. This suggests that this wavenumber k_c is more appropriate than k_d for the upper end of the inertial subrange. Also it is found that $k_d\propto 2^{D/2}$, which has a simple meaning that the dimension of the attractor increases in proportion to the size of the inertial subrange.

An outstanding feature of the Lyapunov exponents is that it has a scaling law; if we plot $\sum_{i=1}^{j}\lambda_i/H$ against j/D for several values of ν, they coincide with each other in the interior of the attractor (i.e., for $j\lesssim D$) except for the first few j's. This scaling law indicates the existence of a normalized form of the distribution function of Lyapunov exponents. The normalized distribution function calculated for several values of viscosity appears to have a singularity around null exponent. This feature can already be recognized in Fig. 4, where a somewhat long flat part of the curve for the intermediate values of j indicates the accumulation of the Lyapunov exponents at $\lambda=0$. On the other hand, the Lyapunov exponents for $j\gtrsim D$ are closely related to the viscous damping rates; $\lambda_{2j}=\lambda_{2j-1}=-\nu k_j^2$. This characterizes the exterior of the attractor.

Let $v_i^{(j)}$ denote the i-th Fourier component of the j-th Lyapunov vector. We

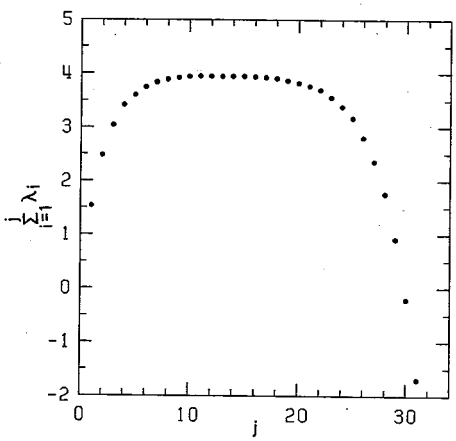

Fig. 4. The cumulated Lyapunov exponents.

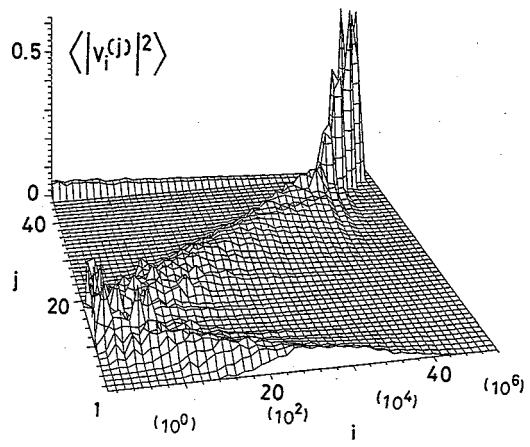

Fig. 5. The time average of the squared components of the Lyapunov vectors $\langle|v_i^{(j)}|^2\rangle$, where i and j respectively represent Fourier and Lyapunov indices. The inertial subrange extends roughly between $i=10$ and 40, while almost null and negative Lyapunov exponents in the interior of the attractor between $j=10$ and $40(\cong 1.3D)$. The numbers in the parentheses denote corresponding wavenumbers.

show in Fig. 5 the time-average of the squared components of the Lyapunov vectors $\langle|v_i^{(j)}|^2\rangle$, where we define $|v_{2i-1}^{(j)}|^2=(\mathrm{Re}\ v_i^{(j)})^2$ and $|v_{2i}^{(j)}|^2=(\mathrm{Im}\ v_i^{(j)})^2$ for $i=1\sim N$, $j=1\sim 2N$.*) Three features should be noted. i) The sharp peaks for $i, j\gtrsim D$ indicate that the Lyapunov and the Fourier bases are frozen to each other (the strong L-F correspondence). ii) In the intermediate wavenumber region, on the other hand, there is a relatively weak but definite correspondence between i and j, indicating that the Lyapunov vector (with $j\lesssim D$) whose Lyapunov exponent is almost null or negative has a support in the inertial range (the weak L-F correspondence). iii) The first Lyapunov vector has its support in the inertial subrange.

§ 3. Intermittent energy transfer

In the previous sections we have discussed the properties of solution of (2·1) from viewpoints of both the classical phenomenological theory (the Fourier perspective) and the dynamical system theory (the Lyapunov perspective) to find a possible relation between the scaling laws of Kolmogorov and Lyapunov spectrum. The relation is global in the sense that it is concerned with the long-time averages of physical quantities. Hereafter we focus our attention on (temporally) local behavior of the solution.

3.1. *Variance of energy flux*

We have seen that the time average of the energy flux is constant in the inertial subrange in Fig. 2. The variance of the energy flux $\langle\varepsilon(k)^2\rangle$ is found, however, to be proportional to $k^{\mu}(\mu\sim 0.3)$ in the same range as in Fig. 6. This means that the fluctuation of the energy flux is larger for higher wavenumber region in the inertial subrange, which indicates that the temporal intermittency of energy transfer is enhanced through the energy cascade process.

In the real fluid turbulence it is often supposed that the energy transfer and energy dissipation rate have the same variance.[10] It follows that the correlation of the energy dissipation rates at two points separated at distance r is proportional to $r^{-\mu}$, where the exponent μ is defined in the same way as above. Through this relation, the value of μ has been experimentally determined to be around 0.2.[11] This value is close to that found in our model. However, this agreement seems to be accidental one. This is firstly because our model is constructed in Fourier space and does not have the physical space where the value of μ is experimentally determined, and secondly because the value of μ is expected to

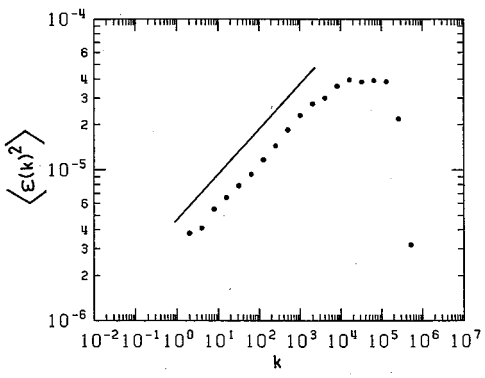

Fig. 6. The variance of the energy flux function. The straight line shows the slope 0.3.

*) A rather long correlation along i-axis in the highest j region is due to numerical error of orthonormalization. Such correlation is not found in computations with fewer modes.

depend on the details of the nonlinear interactions of the Navier-Stokes equation.[12] But we cannot rule out completely the possibility that the intermittency exponent μ has a simple origin in the energy cascade process and is universal in some sense.

3.2. *Instantaneous energy flux*

The above results remind us of the works of Siggia,[13] in which he investigated the intermittency on a cascade model. (His model does not explicitly show the K41 scaling nor intrinsic stochasticity.) He proposed an interesting view of intermittency that the energy propagates in the inertial subrange in the form of wavepackets (in wavenumber space) which occur randomly. This idea has been extended by several authors.[14]

We show below that such a view is basically correct so far as our model is concerned. In Fig. 7(a), the instantaneous energy flux is shown from $t=320$ to $t=323$ with equal time separation 0.05, and those from $t=323$ to $t=326$ are plotted in Fig. 7(b). In the former the energy transfer is limited to the lower wavenumber region and is not effective in the inertial subrange, while in the latter the energy transfer propagates through the inertial subrange like bursts. We will call the former "the quiescent phase" and the latter "the activated phase". Throughout both the phases the energy flux is almost always positive. In the activated phase, the maximum energy flux is about 50 times as large as the mean value. We give in Fig. 8 the perspective view of the energy flux from $t=320$ to 326, which shows temporal intermittency in the energy cascade process in an intuitive way.

The energy transfer process is a mixture of the quiescent and the activated phases. To see how the wavepackets in the activated phase behave, we plot on the k-t plane the location of the maxima of $(\varepsilon(k)-\langle\varepsilon(k)\rangle)/\sqrt{(\langle\varepsilon(k)^2\rangle-\langle\varepsilon(k)\rangle^2)}$ in Fig. 9, where the location of the maximum points of the energy flux thus determined is shown for $t=300\sim400$. This figure shows that such bursts occur randomly and are separated by rather long quiescent phases. Note that this quiescent phase is comparable to the large-scale turnover time $\tau(k_f)$ of order 10, where $k_f=1$ is the forced mode wavenumber (see Fig. 3). We also see that the loci of peaks are upwardly convex

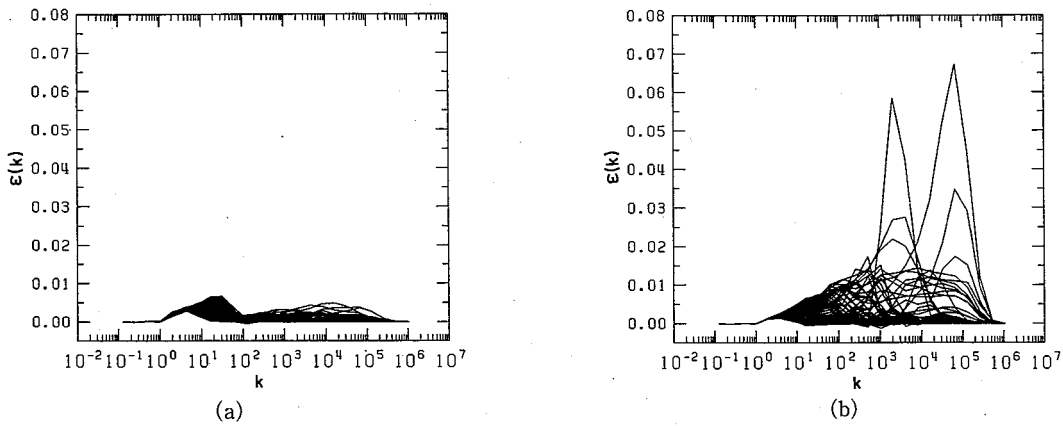

Fig. 7. (a) The instantaneous energy flux function from $t=320$ to 323; the quiescent phase.
(b) The instantaneous energy flux function from $t=323$ to 326; the activated phase.

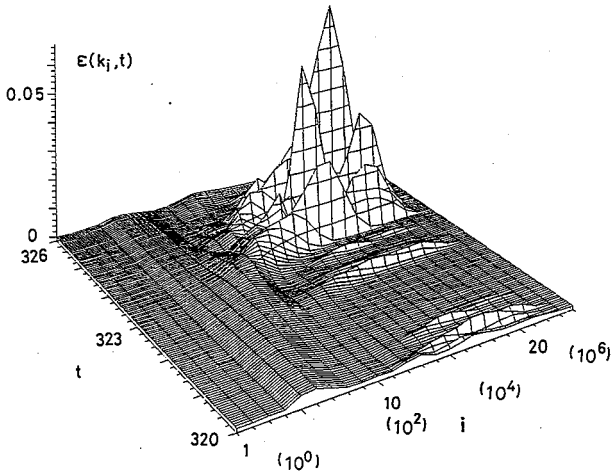

Fig. 8. The perspective view of the energy flux function from $t=320$ to 326. The numbers in the parentheses denote corresponding wavenumbers.

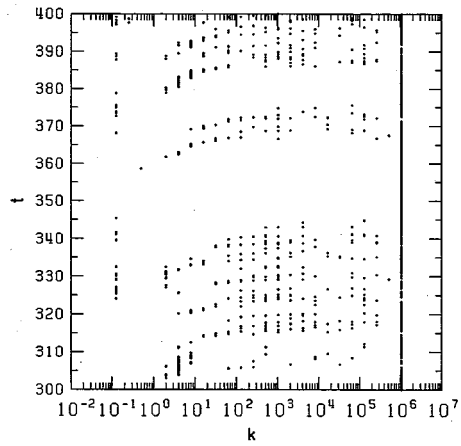

Fig. 9. The location of the peaks of energy flux on k-t plane.

curves, which is consistent with smaller time scales in higher wavenumber regions.

3.3. *Speed of bursts*

It is generally conjectured, but is not proved, that the solution to 3D Euler equation will in general blow up in a finite time, even though the initial condition is smooth. There is a heuristic argument to explain the ill-posedness in terms of wavepacket behavior.[15] Let the characteristic wavenumber of the wavepacket be $K(t)$, and the dimensional argument of Kolmogorov type gives

$$dK(t)/dt \sim \varepsilon^{1/3} K(t)^{5/3} . \tag{3·1}$$

In the inviscid case, the wavepacket thus will reach infinite wavenumber in a finite time t^* as $K(t) \sim (t^* - t)^{-3/2}$, which indicates a finite amount of energy reaches inifinite wavenumber in a finite time; the blowup of the solution.

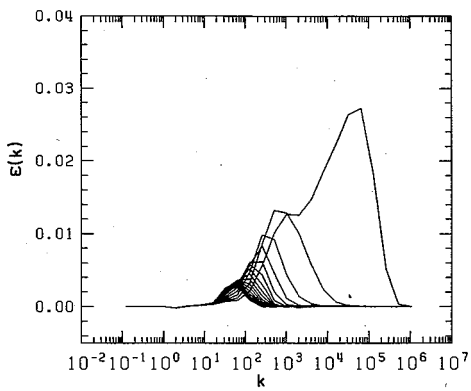

Fig. 10. The instantaneous energy flux function from $t=340$ to 340.75, showing that the peak moves faster in the higher wavenumber regions.

In Fig. 10 an example of wavepacket propagation is shown for $t=340 \sim 340.75$. This, and also Fig. 9, show that the energy propagates faster and faster as it goes through the inertial subrange. The above simple argument gives $t - t^* \sim \exp[-2/3 \log(K(t))]$, which shows that the convex loci on the k-t plane were exponential. But we cannot conclude that $K(t)$ has precisely the same time-dependence as above because of the discretization of the wavenumber space in octaves.

§ 4. Local Lyapunov analysis

In this section we interpret the temporal intermittency observed in § 3 in terms of local Lyapunov analysis.

4.1. *Local Lyapunov exponents*

The Lyapunov spectrum $\{\lambda_j | j=1\sim N\}$ introduced in § 2.3 measures the divergence rates of nearby trajectories in the long-time average on a strange attractor and it does not describe temporal fluctuations of the divergence rate. Therefore it is worth while to introduce some quantity characterizing the temporally local behaviors as observed in the previous section. Here we employ the j-th *local Lyapunov exponent* or the local divergence rate averaged in a short interval $[t, t+\Delta t]$ defined by

$$\mu^{(j)}(t)=1/\Delta t \cdot \log[|\boldsymbol{v}^{(j)}(t+\Delta t)|/|\boldsymbol{v}^{(j)}(t)|], \qquad (4\cdot1)$$

where $\boldsymbol{v}^{(j)}$ is the j-th Lyapunov vector and $|\cdot|$ denotes the norm of the energy type. Numerically Δt is chosen as some multiple of the time spacing between the orthonormalization procedures. Here we take $\Delta t=0.05$ which is small compared to eddy turnover time $\tau(k)$ in the inertial subrange. Note that we can recover the (ordinary) Lyapunov exponents by averaging Eq. (4·1) over t; $\lambda_j=\langle\mu^{(j)}(t)\rangle$. Also, we define the variance of $\mu^{(j)}(t)$ by $\sigma_j^2=\langle\mu^{(j)}(t)^2\rangle-\langle\mu^{(j)}(t)\rangle^2$.

We mainly consider the first local

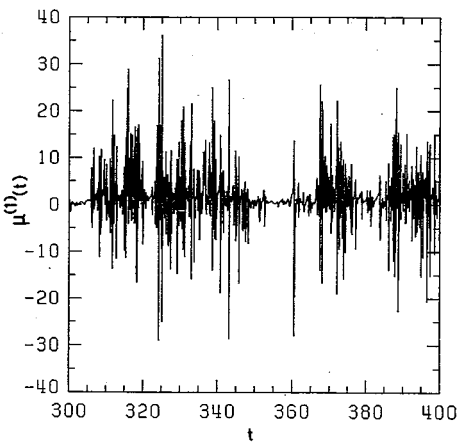

Fig. 11. The first local Lyapunov exponent.

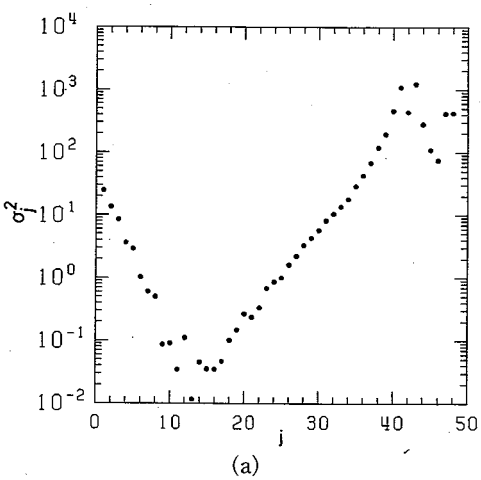

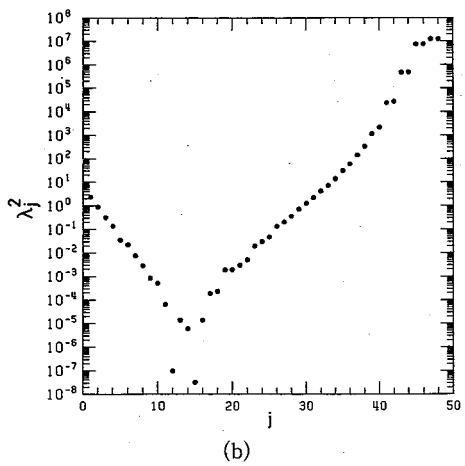

Fig. 12. (a) The variance of the Lyapunov exponents.
(b) The squared Lyapunov exponents.

Lyapunov exponent. We show the time evolution of $\mu^{(1)}(t)$ from $t=300$ to 400 in Fig. 11. In this figure we see highly irregular behavior of $\mu^{(1)}(t)$, which is interrupted by quiescent periods. Their peaks are as large as ± 30, indicating large fluctuations compared to the mean value $\lambda_1=1.54$.

Comparison between Figs. 9 and 11 shows that in the quiescent periods of $\mu^{(1)}(t)$ no peaks of energy flux are found in the inertial subrange, and that when $\mu^{(1)}(t)$ behaves like bursts, the peaks of energy flux lie in the inertial subrange.*)

The variance of the local Lyapunov exponents σ_j^2, which may be a couterpart of variance of the energy transfer rate, is shown in Fig. 12(a). Remember that the Lyapunov exponents λ_j for $j \leqq 10$ are positive while those for $j \geqq 11$ are negative. We can see that the variance of the local Lyapunov exponents has a scaling law in the interior of the attractor as $\sigma_j^2 \propto e^{aj}$ for $j \geqq 11$ ($a \sim 0.24$) and $\sigma_j^2 \propto e^{-bj}$ for $j \leqq 10$ ($b \sim 0.54$). The variance of the local Lyapunov exponents therefore reaches minimum around $\lambda \sim 0$. We also show the squared Lyapunov exponents in Fig. 12(c). In the exterior of the attractor they come out in pairs (the strong L-F correspondence). In the interior of the attractor they behave as $\lambda_j^2 \sim e^{a'j}$ for $j \geqq 11$ ($a' \sim 0.62$) and $\lambda_j^2 \sim e^{-b'j}$ for $j \leqq 10$ ($b' \sim 0.99$). Thus the normalized variance σ_j^2/λ_j^2 reaches maximum around $\lambda \sim 0$. These results suggest that not only the Lyapunov exponents but also their variances have a scaling property of the exponential form.

4.2. *Instantaneous Lyapunov vectors*

The direction of the first Lyapunov vector is the most unstable direction. We show in Fig. 13 the location of the maxima of the squared components of the first Lyapunov vector $|v_i^{(1)}|^2$ at each instant of time. These peaks generally distribute over the inertial subrange, so that the correspondence between the dominant components of the first Lyapunov vector and the peaks of energy flux is less clear than the correspondence found in § 4.1. Nevertheless by comparing Fig. 13 with Fig. 9, we find that the first Lyapunov vector lies in the inertial subrange when the energy transfer occurs in the activated phase. In the quiescent phase, on the other hand, the first Lyapunov vector is localized in the lower wavenumber region like the energy flux function.

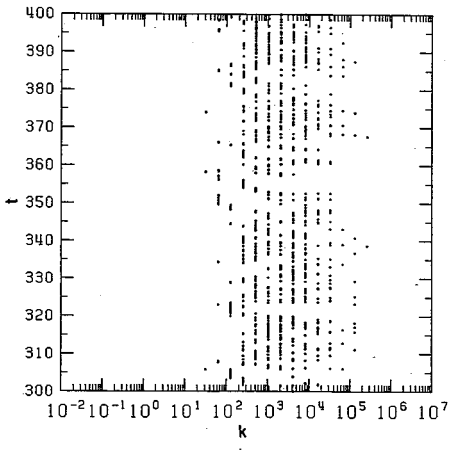

Fig. 13. The location of the peaks of the first Lyapunov vector.

4.3. *Conditional averages*

Let us consider the conditional averages of the local Lyapunov exponent in the activated and quiescent phases. Normalizing the first local Lyapunov exponent as $\xi_1(t)=(\mu^{(1)}(t)-\langle\mu^{(1)}(t)\rangle)/\sqrt{\langle(\mu^{(1)}(t)-\langle\mu^{(1)}(t)\rangle)^2\rangle}$, we define the

*) Similar correspondence has been found in the Kuramoto-Sivashinsky equation by Professor K. Ikeda (private communication).

Table I. The conditional average of the local Lyapunov exponents. For each threshold value α, the local Lyapunov exponent averaged in the activated phase λ_A and the rate of the activated phase r_A to the total time duration are given. Similarly λ_Q and r_Q are presented.

α	λ_A	$r_A(\%)$	λ_Q	$r_Q(\%)$
0.1	1.55	82.83	1.51	17.17
0.3	1.94	46.27	1.19	53.73
1.0	2.78	16.18	1.30	83.82
2.0	3.19	6.02	1.43	93.98

activated phase by $A(\alpha)=\{t:|\xi_1(t)|>\alpha\}$ and the quiescent phase by $Q=\{t:|\xi_1(t)|<\alpha\}$ for a threshold value α. The conditional average of the first local Lyapunov exponent in the activated phase is then defined by $\lambda_A=\langle\mu(t)\rangle_A$, where time average is taken in $A(\alpha)$. We can similarly define $\lambda_Q=\langle\mu(t)\rangle_Q$. The results for $\alpha=0.1, 0.3, 1.0, 2.0$ are summarized in Table I. We note that not only λ_A but also λ_Q is positive: λ_A is only slightly larger (roughly by a factor of 2) than λ_Q for $\alpha>1$. This means that there is divergence of nearby trajectories in the phase space not only in the activated phase but also in the quiescent phase.

The Lyapunov vectors shown in Fig. 5 are the long-time average which neglect the difference between the activated and quiescent phases. To see how the structure of the Lyapunov vectors changes in these two phases, we consider the conditional average of the squared components of the Lyapunov vectors $\langle|v_i^{(j)}|^2\rangle_A$ in the activated phase and $\langle|v_i^{(j)}|^2\rangle_Q$ in the quiescent phase. We show them respectively in Figs. 14(a) and (b) using $\alpha=1$. (See the footnote on p. 334.) The result with $\alpha=2$ is qualitatively the same. Comparing these to the global average $\langle|v_i^{(j)}|^2\rangle$ (Fig. 5), we find out that the first Lyapunov vector in the activated (quiescent) phase lies in the higher(lower) wavenumber region than the global average. This is consistent with the property discussed in § 3.3; the support of the first Lyapunov vector lies in the lower wavenumber region in the quiescent phase than in the activated phase.

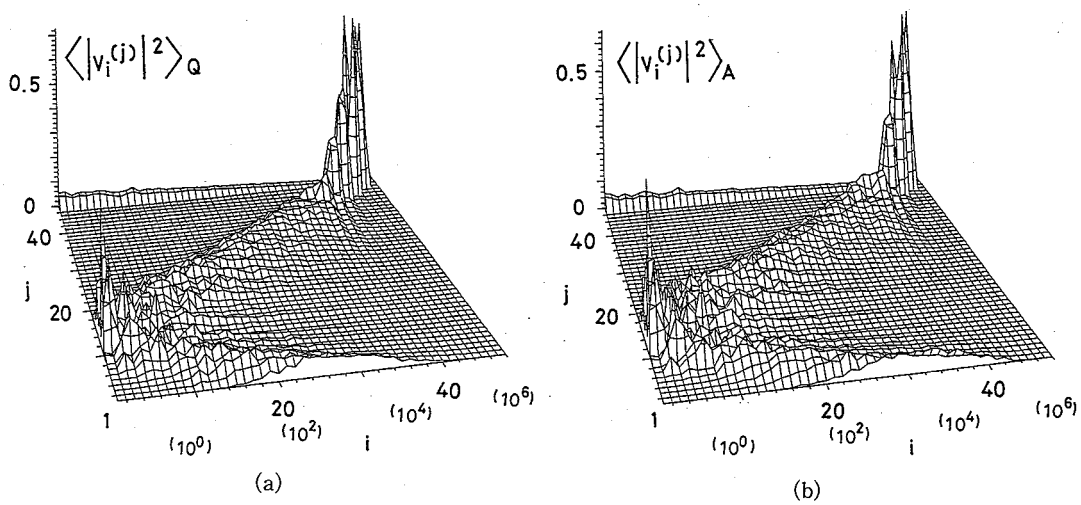

Fig. 14. (a) The squared components of the Lyapunov vectors averaged in quiescent periods $\langle|v_i^{(j)}|^2\rangle_Q$, where i and j respectively represent Fourier and Lyapunov indices. The numbers in the parentheses denote corresponding wave numbers.

(b) The squared components of the Lyapunov vectors averaged in activated periods $\langle|v_i^{(j)}|^2\rangle_A$, where i and j respectively represent Fourier and Lyapunov indices. The numbers in the parentheses denote corresponding wave numbers.

In the highest wavenumber region ($i, j > 40$, the wavenumber region of the strong L-F correspondence) we see very sharp peaks both in the activated and quiescent phases, indicating that the corresponding Fourier and Lyapunov bases are always frozen to each other.

In the intermediate range $10 < i, j < 40$, the inertial subrange in the Fourier perspective corresponds to the interior of the attractor in the Lyapunov perspective (the weak L-F correspondence). The weak L-F correspondence is relevant to the nonpositive Lyapunov exponents which are related to the stability of the motion. However, we note that the weak L-F correspondence persists not only in the quiescent phase but also in the activated phase. Therefore, the characterization of the inertial subrange by the weak L-F correspondence turns out to be phase independent.

§ 5. Summary and discussion

Employing a particular cascade model of turbulence, we have discussed temporal intermittency of the energy cascade process in connection with local Lyapunov analysis. Time development of the model turbulence consists of two parts; the activated phase and the quiescent phase. In the activated phase, the energy cascade occurs like bursts and the first local Lyapunov exponent oscillates violently. Simultaneously the support of the first Lyapunov vector distributes over the inertial subrange. In the quiescent phase, the energy cascade process is scarcely effective and (the first) local Lyapunov exponents behave mildly with the Lyapunov vector localized in the lower wavenumber range.

Thus, so far as the present model is concerned, the energy cascade process in the inertial range can be characterized in the Lyapunov perspective not only by its averaged property but also by its fluctuations from it. The former is the characterization of the inertial subrange by the weak L-F correspondence.[4] This is connected with almost null and negative Lyapunov exponents in the interior of the attractor. This connection holds independently of whether the phase is quiescent or activated. The latter characterization is connected with the first Lyapunov vector; the inertial subrange is the support of the first Lyapunov vector. This is related to the instability of the system in contrast to the former characterization.

The present model shares some fundamental properties with the 3D Navier-Stokes equation, but still there are profound differences between them. For example, the 3D Navier-Stokes equation has a huge number of modes, vectorial quantities, physical space characteristics and so on. The energy transfer process in the 3D wavenumber space is much more complex than that in the 1D discretized wavenumber space. Especially, the intermittency phenomenon will be not only temporal but also spatial. But the fluctuations around the averaged properties, which we are mainly concerned with in this paper, are interesting quantities also in real fluid turbulence. We expect that some of the present results will be helpful for understanding Navier-Stokes turbulence, especially when we investigate it with an emphasis on temporal intermittency.

We can also study the enstrophy cascade process on Gledzer's model of 2D turbulence by the same methods as in this paper. The dynamics of the enstrophy

cascade is found quite different from that of energy cascade. Details of the study will be reported elsewhere.

Acknowledgements

The authors have benefitted from discussions with Professor K. Ikeda and Professor S. Kida. They also express their cordial thanks to Professor T. Kawahara and Dr. S. Toh for helpful comments. Thanks are also due to Professor T. Tatsumi for encouragement.

References

1) J. P. Eckmann and D. Ruelle, Rev. Mod. Phys. **57** (1985), 617.
2) A. N. Kolmogorov, CR Acad. Sci. **30** (1941), 301.
3) M. Yamada and K. Ohkitani, J. Phys. Soc. Jpn. **56** (1987), 4210.
4) M. Yamada and K. Ohkitani, Prog. Theor. Phys. **79** (1988), 1265.
5) V. N. Desnyansky and E. A. Novikov, Prik. Mat. Mekh. **38** (1974), 507.
T. L. Bell and M. Nelkin, J. Fluid Mech. 88 (1978), 369.
6) R. Grappin, J. Leorat and A. Pouquet, J. de Phys. **47** (1986), 1127.
7) S. A. Orszag, *Lectures on the Statistical Theory of Turbulence in Fluid Dynamics, Les Houches, 1973,* ed. R. Balian and P. L. Peube (Gordon and Breach, New York, 1977), p. 235.
8) E. B. Gledzer, Sov. Phys.-Dokl. **18** (1973), 216.
9) M. Yamada and K. Ohkitani, Phys. Rev. Lett. **60** (1988), 983.
10) U. Frisch, P.-L. Sullem and M. Nelkin, J. Fluid Mech. **87** (1978), 719.
11) F. Anselmet, Y. Gagne, E. J. Hopfinger and R. A. Antonia, J. Fluid Mech. **140** (1984), 63.
12) R. H. Kraichnan, J. Fluid Mech. **62** (1974), 305.
13) E. D. Siggia, Phys. Rev. **A15** (1977), 1730; **A17** (1978), 1166.
14) T. Nakano and M. Nelkin, Phys. Rev. **A31** (1985), 1980.
T. Nakano, Prog. Theor. Phys. **75** (1986), 1295.
15) T. Nakano, Prog. Theor. Phys. **73** (1985), 629.